Article

Application of Factorial Analysis to the Study of Vented Dust Explosions in Large Biomass Storage Silos

Alejandro Varela [1], Julia Arbizu-Milagro [1] and Alberto Tascón [1,2,*]

1   Department of Agriculture and Food Science, Universidad de La Rioja, Av. Madre de Dios 53,
26006 Logroño, Spain
2   CIVA Research Center, Universidad de La Rioja, 26006 Logroño, Spain
*   Correspondence: alberto.tascon@unirioja.es

Abstract: Dust explosions are a major concern in many industrial facilities and particularly in storage areas of biomass materials. Although venting standards (EN 14491 and NFPA 68) provide satisfactory safety levels for most industrial applications, they present some limitations and there exist situations that they do not contemplate. Vented dust explosions in a 4500 m^3 silo for the storage of wood pellets were simulated by computational fluid dynamics. Maximum overpressures were registered and compared. The influence of several parameters including initial turbulence level, dust concentration, ignition location, and vent area was studied. A factorial analysis was carried out to determine the importance of each of the four parameters, along with possible interactions between them. The results showed great variations in the overpressures between the different scenarios simulated. Vent area, ignition location, and dust concentration showed similar effects on the overpressure (around 25%), while initial turbulence had half this effect (13%). One interaction effect out of the eleven possible interactions was identified as relevant for this specific industrial scenario: the combination of the ignition location and the initial turbulence, with an additional effect of 5% on the overpressure. The factorial analysis applied in this study could be of interest to the risk assessment of industrial facilities.

Keywords: dust explosion; venting; silo; CFD; wood pellets; explosion safety; explosion mitigation

1. Introduction

Dust explosions represent a main concern in the industries that handle, process, or store combustible materials that produce fine particles [1]. If these particles are suspended in air due to the movement of the bulk material during transport or conditioning operations (sieving, milling, etc.) [2] or due to the dust lifting from layers and deposits [3] caused by an airflow, pressure wave or vibrations, a rapid combustion process can be triggered by an ignition source with enough energy. This results in the propagation of a flame through the dust/air mixture and the generation of heat and gaseous products, which can produce important overpressures when the explosion occurs within a confined space [4].

This phenomenon has been reported in different types of industrial facilities and equipment, such as dust-collecting systems, dryers, conveyors, and silos. Among them, storage silos for bulk materials represent one of the most common equipment types involved in dust explosion accidents [5].

Hot surfaces and hot lumps of material, mechanical sparks, electric sparks and electrostatic discharges, lightning, and welding and cutting operations are well-known potential ignition sources [6]. In addition, fires –both open flame fires and smoldering fires– can ignite a dust explosion [6]; these fires can be the result of a self-heating process undergone by the bulk material [7] and the emission of flammable volatiles [8]. Similarly, flames by dust explosions could produce subsequent fires in surrounding facilities, buildings, and vegetation if not addressed properly.

Dust explosions represent a significant percentage of the major accidents in the biomass and bioenergy sector [9]. Safety concerns in biomass storage facilities deserve further attention [10]. Particularly, large storage silos for wood pellets are common in biomass power plants, co-firing installations, harbor storage areas, and pellet-manufacturing industries. Therefore, these storage facilities are exposed to explosion risks that should be assessed, managed, and mitigated [11].

Mitigation of dust explosions involves several measures [4] but venting is one of the most popular. Pressure relief or venting consists of allowing explosion gases to escape from the equipment to be protected in order to limit the overpressures generated by the explosion to a level that the equipment can withstand [12]. Venting safeguards the equipment and prevents its bursting, which would eject wall fragments, burning material, hot ashes, and unburned material; this late situation should be avoided to reduce fatalities and prevent subsequent fires and a possible domino effect in the industrial facility [13]. Therefore, venting reduces the potential damage caused by explosions but neither prevents nor extinguishes an explosion.

Standards for dust explosion venting (EN 14491 [14] and NFPA 68 [15]) are based both on theoretical considerations and empirical data. These data were mainly obtained from experimental programs conducted during the 60's–90's decades of the 20th century. These standards provide the total vent area required to achieve proper protection of vessels in the event of an internal dust explosion. Both methods are conservative and lead to satisfactory safety levels for most industrial applications since they were developed assuming a homogeneous turbulent dust cloud filling the vessel to be protected [16,17].

The formulae proposed in both standards [14,15], for the simplest scenario, consider a number of parameters related to the dust (the K_{St} constant in bar·m·s^{-1} and the maximum explosion overpressure P_{max} in bar, both determined through laboratory experiments [18,19]), the vessel to be protected (the volume V in m^3, the length-to-diameter ratio L/D, and the maximum explosion pressure in bar that the vessel can withstand, also named reduced overpressure P_{red}), and the venting devices (the static activation pressure of the venting devices P_{stat} in bar, the venting efficiency or inertia, and the presence or not of a duct).

However, venting protection remains a complex issue due to frequent technical and economic difficulties [20]. The above standards calculate such large vent areas in some cases–particularly in low-strength vessels of large volume, such as large steel silos–that they are difficult to implement in practice [21]. Moreover, they do not consider other process or design variables different than those listed above but that could also have an important effect on the venting process. In this sense, it is remarkable that Middha et al. [22] demonstrated by means of numerical simulations that the layout of the vent panels influences the explosion overpressure due to the interaction of flame jets between vent zones and the subsequent reduction in venting efficiency. In addition, standards have a specific range of applications [20]; Coffey and Price [11], for instance, studied a silo with a volume of 101,000 m^3, which falls outside of the scope of the standards. Tascón and Aguado [23] also analyzed cases not contemplated by standards conducting both simulations and experimental explosions in a 5 m^3 vessel; they demonstrated the influence of the activation pressure of the vent panels and of the relation $V^{2/3}/A$ (cross-sectional area of a cube with equivalent volume divided by the vent area) on the explosion overpressure. Other aspects that have recently been discussed due to the significant uncertainties still present include the role of turbulence [24], the influence of the length-to-diameter ratio of the vessel [25,26], and the relief through vent ducts [27].

Therefore, it is clear that there is ample room for improvement in the methodologies employed in explosion relief design. There are various factors, design choices, and real industrial scenarios that cannot be properly assessed using the current venting standards, which only consider some specific situations covered by the experiments they are based on. In this sense, numerical simulations are a powerful tool and allow practitioners and researchers to analyze a wider range of possible initial scenarios. Computational fluid

dynamics (CFD) codes have already been successfully applied to dust explosions, including aspects like the turbulent concentration field [28,29], the dust lifting phenomenon [3], interconnected vessels [30,31], the investigation of real accidents [32], and the protection of industrial equipment against dust explosions [11,33–35]; other types of explosions have also been studied by means of CFD simulations [36,37].

The objective of this study was to perform numerical simulations of vented dust explosions in a biomass storage silo in order to analyze the effects of variations in the initial scenario and the influence of the parameters involved. The importance of each parameter and the interactions between them were also studied.

2. Materials and Methods

2.1. CFD Code

The FLACS-CFD v22.1r2 software from Gexcon, equipped with the specific FLACS-DustEx solver, was utilized for conducting the dust explosion simulations [38].

This software is a finite volume code that solves the conservation equations on a 3-D Cartesian grid. Turbulence is solved by using a Reynolds-averaged Navier-Strokes k–ε model, and the SIMPLE pressure correction algorithm is applied [39]. FLACS-CFD models curved surfaces and subgrid obstacles using a distributed porosity approach, where volume and area porosities (or fractions) are calculated on the cells of the mesh and included in the conservation equations, ranging from 0.0 (100% solid cell) to 1.0 (100% fluid cell) [40]. A detailed description of the governing equations of the code has already been reported and can be found in [41].

The combustion model implemented in the code determines the reaction rate from reactants to products and the propagation of the reaction zone, i.e., the flame. The approach adopted in FLACS-DustEx to calculate the burning velocity of the dust/air mixture in turbulent conditions (S_T) consists of applying Equation (1) using the laminar burning velocity (S_L) values estimated from experimental data measured in the 20-L vessel [18] for several concentrations. The estimates of the laminar burning velocity can be augmented C_L times, being C_L a correction factor introduced to account for the uncertainties behind the calculations. In addition, the experimental explosions in the 20-L vessel also provide the mass fraction of fuel converted to products (λ) for various dust concentrations, which is calculated from the explosion overpressure recorded in the 20-L vessel considering the fuel that must react with air to produce that pressure, prior correction to account both for the igniters and for the cooling effects of vessel walls. Finally, the S_L and λ data for different concentrations are stored in a text file that is used as input for the combustion model. A complete description of the derivation of S_L and λ from the experimental data was reported by Skjold [42,43].

$$S_T = 15.1 \, S_L{}^{0.784} \, u'_{rms}{}^{0.412} \, l_I{}^{0.196}, \tag{1}$$

where u'_{rms} is the root-mean-square of the turbulent velocity fluctuations and l_I is the turbulence length scale.

2.2. Scenario

The simulated industrial equipment comprised a wood pellet storage silo with a capacity of 4500 m^3. The silo had a cylindrical body with inner dimensions of 20 m in diameter and 13 m in height, plus a conical roof that added 8 m in height. The computational domain occupied a floor area of 48 × 48 m^2 and 52 m in height (volume = 119,808 m^3). The domain was discretized into a uniform grid composed of cubic cells measuring 1 m in size. To adapt the conical roof to the orthogonal grid used by FLACS-CFD, the roof was transformed into a series of toroids with decreasing diameter (see Figure 1). Three monitoring points (MP) were positioned along the vertical *z*-axis of the silo at heights of 2.25 m (MP-1), 13.25 m (MP-2), and 20.25 m (MP-3) from the silo bottom. However, to avoid alignment with grid lines, a small deviation of −0.25 m was introduced in both the *x*- and *y*-axes.
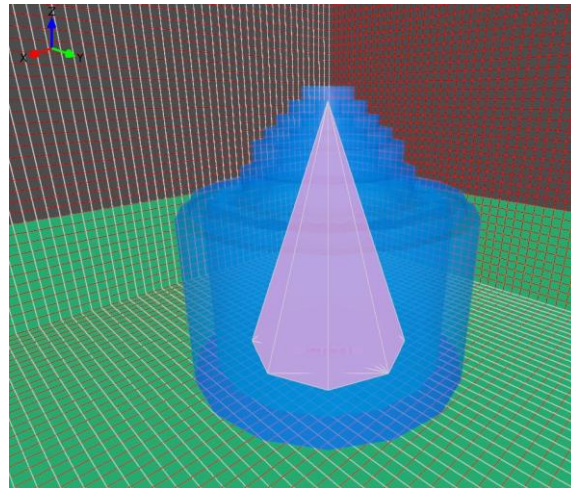
Figure 1. The geometric configuration of the silo and inner dust cloud.

For the simulations it was assumed that the silo was empty of bulk material, i.e., the entire volume was filled with either air or dust/air mixture. The initial pressure was set at 100 kPa, and the initial temperature was 20 °C. The initial dust cloud used in these simulations had a pyramidal shape and occupied the entire height of the silo, from the top of the roof down to the bottom (see Figure 1). This cloud had a volume of 980 m^3, representing only a fraction of the silo's internal volume (21.8%).

This approach tried to replicate a realistic scenario during the initial phase of the filling process: the material (wood pellets) would fall from a conveyor situated above the silo generating a dust cloud that would follow the trajectory of the pellets and widen at the silo bottom. A uniform dust concentration was considered in all the volume of the cloud. Wood dust was used in all the simulations (P_{max} = 7.9 bar for 500 g/m^3 and K_{St} = 131 bar·m/s for 1000 g/m^3, determined following standardized procedures [18,19]).

Pressure relief panels were included in the roof, each one measuring 1 × 1 m^2, inertia-less, and with an activation pressure of 0.1 bar (gauge pressure). The panels were uniformly distributed around the larger toroid of the roof in all simulations. Some simulations were performed employing 56 panels (see Figure 2) and others using 28.
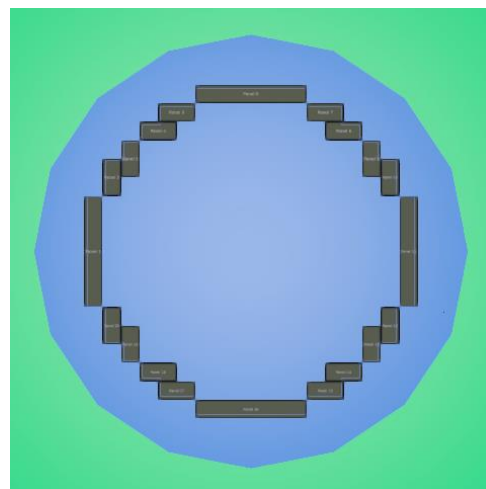

Figure 2. Top view of the silo showing the pressure relief panels with a total area of 56 m^2.

2.3. Factorial Design

The study aimed to discover the effect of different possible initial conditions on the reduced explosion overpressures reached inside the silo ($P_{red,sim}$) during a vented dust

explosion. From the whole set of parameters that could modify the explosion development, 4 factors with 2 levels each were chosen. The factors involved in this study were vent area, ignition location, initial turbulence, and dust concentration.

2.3.1. Vent Area

Vent area refers to the total surface area provided by the venting devices installed in the roof in order to protect the silo from explosion overpressures. This factor reflects the vent area that would open during an explosion. The two levels considered in the simulations were 56 m^2 and 28 m^2.

2.3.2. Ignition Location

Ignition location refers to the specific point within the dust cloud where the ignition was initiated by an energy source. The ignition energy was set to 1 kJ.

The two levels were the following:

- Top: ignition in the upper third of the cloud height (at 19.75 m above the silo bottom);
- Bottom: ignition in the lower third of the cloud height (at 1.25 m above the silo bottom).

Both locations were positioned along the vertical z-axis of the silo but with a small deviation of -0.25 m in the x- and y-axes to avoid contact with the walls of the grid cells.

2.3.3. Initial Turbulence

FLACS-CFD utilizes three parameters to characterize the turbulence level in the initial fluid flow before the explosion: characteristic velocity, relative turbulence intensity, and turbulence length scale.

The two levels were as follows:

- Low: the three parameters had lower values, resulting in weak initial turbulence.
- High: this corresponded to a more severe turbulent flow.

The specific values for the two initial condition sets are shown in Table 1. In the low-level scenario, the air velocity and relative turbulence intensity are based on experimental measurements carried out by Hauert et al. in a 12 m^3 silo when fed mechanically with maize starch [44]. These low-level values have been used in previous simulations [34] and were obtained by considering average numbers for the entire volume and making adjustments to account for the volume increase. Further discussion on these aspects can be found in [34].

Table 1. Turbulence initial conditions.

Level	Characteristic Velocity (m/s)	Relative Turbulence Intensity	Turbulence Length Scale (m)
Low	0.15	0.80	0.03
High	0.50	1.00	0.10

2.3.4. Dust Concentration

Dust concentration represents the quantity of combustible dust in the homogeneous dust/air cloud formed into the vessel, expressed in g/m^3. The two levels were set at 300 g/m^3 and 500 g/m^3. The latter was the concentration that generated the maximum overpressure (P_{max} = 7.9 bar) in the 20-L vessel [18], while the former was based on measurements in an experimental silo [44]. These two values have already been used in previous CFD simulations [34,41].

2.4. Factorial Analysis

A 2^k factorial analysis [45] was applied to determine the influence of the factors on $P_{red,sim}$, as well as to examine potential interactions between the factors.

The levels of each factor were assigned values -1 or $+1$, as indicated in Table 2. These values were used to generate all possible combinations of factors and levels, as shown in

Table 3. In this study, 4 factors with 2 levels resulted in a total of 16 different cases. The factors were denoted with letters A, B, C, and D.

Table 2. Levels of the four factors.

	A (Vent Area)	B (Ignition Location)	C (Initial Turbulence)	D (Dust Concentration)
−1	56 m^2	Top	Low	300 g/m^3
+1	28 m^2	Bottom	High	500 g/m^3

Table 3. Combinations of levels for the 4 factors.

Case	A	B	C	D
01	−1	−1	−1	−1
02	−1	−1	−1	+1
03	−1	−1	+1	−1
04	−1	−1	+1	+1
05	−1	+1	−1	−1
06	−1	+1	−1	+1
07	−1	+1	+1	−1
08	−1	+1	+1	+1
09	+1	−1	−1	−1
10	+1	−1	−1	+1
11	+1	−1	+1	−1
12	+1	−1	+1	+1
13	+1	+1	−1	−1
14	+1	+1	−1	+1
15	+1	+1	+1	−1
16	+1	+1	+1	+1

The statistical model for the 2^4 design included 4 main effects (A, B, C, and D), 6 two-factor interactions (AB, AC, AD, BC, BD, and CD), 4 three-factor interactions (ABC, ABD, ACD, and BCD), and one four-factor interaction (ABCD). The contrast coefficients used in estimating the factorial effects–both the main effects and the interaction effects–were selected following the rules reported by Montgomery [46] for a single replicate of the 2^4 design.

The factorial analysis required the calculation of the q, Q, and Y values for the 4 main effects and the 11 interactions:

- q: the sum of the products of $P_{red,sim}$ and the corresponding contrast coefficient, considering the 16 cases;
- Q: calculated as q divided by the number of cases (16);
- Q^2: the square of Q (the total Q^2 is the sum of all Q^2 values);
- Y: the percentage of each Q^2 in relation to the total Q^2.

3. Results

Table 4 shows the maximum values of the explosion-reduced overpressures obtained in the CFD simulations ($P_{red,sim}$). The cases have been ordered from lowest to highest $P_{red,sim}$. According to standards [14,15,18,19], all pressures are expressed in bars throughout the manuscript. Gauge pressure is used in all tables and figures.

The maximum values were recorded at MP-3 in all cases except for case 03 at MP-1. Thus, almost all maximum overpressures were obtained near the silo roof. The mean $P_{red,sim}$ was 0.670 bar but the standard deviation achieved 0.481, i.e., the pressures varied a lot between cases, presenting a very high coefficient of variation of 72%.

Then, the values of $P_{red,sim}$ were grouped by intervals into the following four pressure classes:

- Class 1: $P_{red,sim} \leq 0.5$ bar;

- Class 2: 0.5 bar < $P_{red,sim}$ ≤ 1.0 bar;
- Class 3: 1.0 bar < $P_{red,sim}$ ≤ 1.5 bar;
- Class 4: 1.5 bar < $P_{red,sim}$.

Table 4 also shows the Class and the level of each of the four factors. Class 1 and Class 2 accounted for almost 70% of the cases. The remaining 30% corresponded to Class 3 and only case 16 was above 1.5 bar (Class 4).

Table 4. Case-by-case variables and reduced explosion overpressures ($P_{red,sim}$) obtained in the simulations.

Case	Vent Area (m²)	Ignition Location	Initial Turbulence	Dust Concentration (g/m³)	$P_{red,sim}$ (Bar)	Class
03	56	Top	High	300	0.108	1
01	56	Top	Low	300	0.155	1
05	56	Bottom	Low	300	0.270	1
02	56	Top	Low	500	0.293	1
04	56	Top	High	500	0.321	1
09	28	Top	Low	300	0.344	1
11	28	Top	High	300	0.439	1
13	28	Bottom	Low	300	0.534	2
07	56	Bottom	High	300	0.578	2
06	56	Bottom	Low	500	0.584	2
10	28	Top	Low	500	0.744	2
15	28	Bottom	High	300	1.067	3
14	28	Bottom	Low	500	1.096	3
12	28	Top	High	500	1.146	3
08	56	Bottom	High	500	1.159	3
16	28	Bottom	High	500	1.878	4

Figure 3 illustrates some examples of the pressure-time curves, one for each of the four classes defined. The curves showed two pressure peaks: the first one corresponds to the activation of the vent panels and the second one is $P_{red,sim}$. The first peak was less apparent for Class 1 and Class 2 since the pressure was hardly reduced after the vent opening and it rapidly continued rising.
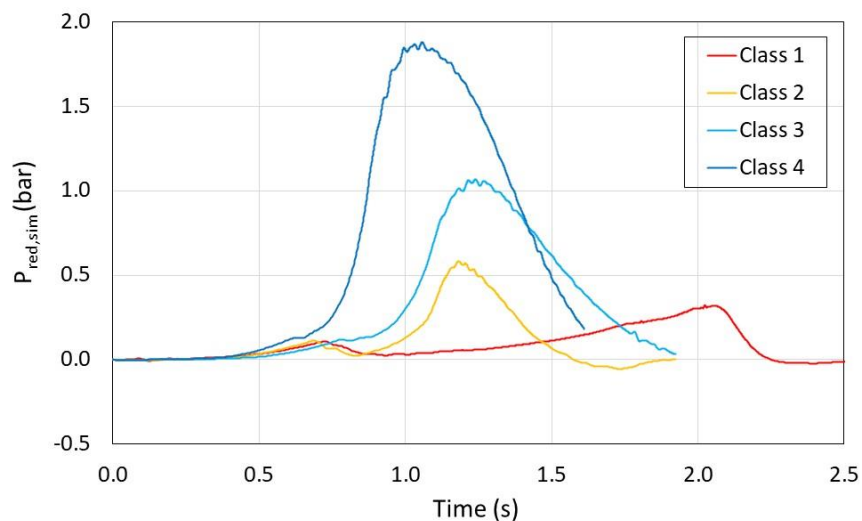

Figure 3. Pressure-time curves at MP-3 for cases 04, 06, 15, and 16 (classes 1, 2, 3, and 4, respectively).

The effect of each factor was studied individually, as well as the 11 possible interaction effects between them. Table 5 provides a summary of the results of this analysis and indicates the most influential effects. As can be seen, vent area, ignition location, and dust concentration had a similar effect on the variation of $P_{red,sim}$, around 25%. In contrast, initial

turbulence had half this effect on $P_{red,sim}$. All values of Q were positive, which means that the levels of the factors assigned with +1 helped to increase the value of $P_{red,sim}$, while those assigned with −1 tended to reduce the value of $P_{red,sim}$.

Table 5. Analysis of the variables.

	A	**B**	**C**	**D**	**BC**
q	3.780	3.616	2.676	3.726	1.720
Q	0.236	0.226	0.167	0.233	0.108
$Q^{2\,(a)}$	0.056	0.051	0.028	0.054	0.012
Y	26%	24%	13%	25%	5%

[a] total Q^2 = 0.217.

One interaction effect out of the 11 possible interactions was identified as relevant: the combination of the ignition location and the initial turbulence (BC), with an additional interaction effect of 5%. Its Q value was positive, i.e., its effect on $P_{red,sim}$ will depend on the two variables following the patterns indicated in Table 6.

Table 6. Interaction effect for ignition location plus turbulence.

Ignition	**Turbulence**	**Additional Effect on $P_{red,sim}$**
−1	−1	Increment
−1	+1	Decrement
+1	−1	Decrement
+1	+1	Increment

The importance of this interaction effect is evident considering that case 01 did not present the lowest pressure even though all its factors were level-1. The additional interaction effect between ignition and turbulence allowed it to have a higher $P_{red,sim}$ than that in case 03.

Finally, results were compared to venting standards [14,15]. Figure 4 illustrates the whole set of simulations, along with the EN 14491 and NFPA curves.
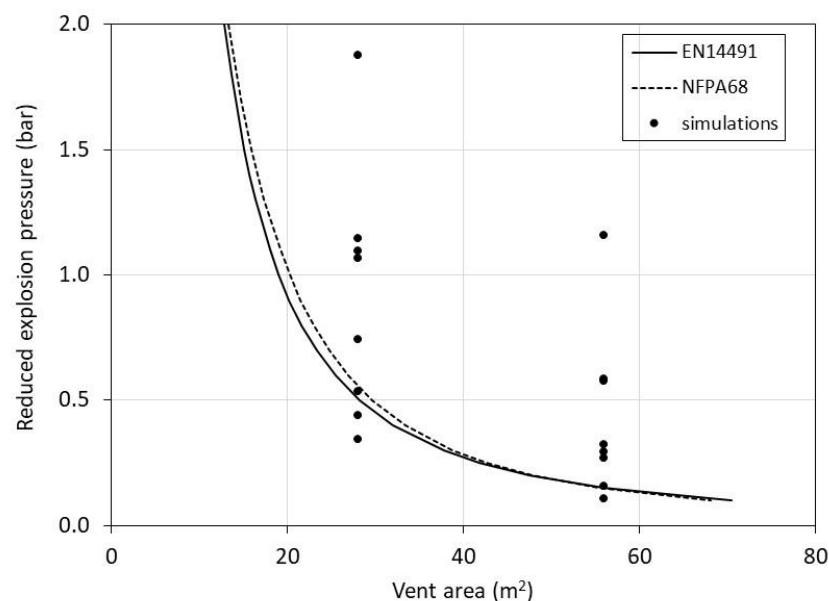

Figure 4. Comparison between the 16 cases simulated with FLACS-DustEx and the EN 14491 [14] and NFPA 68 [15] venting standards.

4. Discussion

The trends that can be drawn from the overpressure results are coherent and match the expected behavior [1]: the higher the turbulence or the dust concentration and the smaller the vent area, the higher the explosion overpressure. On the other hand, a comparison between the cases with different ignition locations indicates that bottom ignition produced overpressures 2.5 times higher on average (maximum = 5.35, minimum = 1.47) than those obtained for top ignition; this tendency was already found by Bartknecht in his 20 m^3 experimental tests [47]. Interestingly, Bartknecht also reported that the pressures measured in the top area of the vessels were higher than those registered in the lower part [47]; as mentioned above, all simulations except one reached their maximum $P_{red,sim}$ in MP-3, which was located near the top of the roof, 20.25 m from the bottom.

The CFD simulations gave huge differences in the reduced explosion overpressure between the different cases considered, all of which represent situations that could happen in reality. As can be seen in Figure 4, some cases were above the venting standards curves, while others were below. It is important to note that the turbulence levels considered here are quite conservative for a large silo with a mechanical filling system. However, pneumatic filling –sometimes used in biomass storage facilities– or extraordinary events, like an external primary explosion entering the silo, could lead to these turbulence levels or even much higher. The importance of turbulence in industrial equipment venting was already highlighted in the pioneering research work by Eckhoff [48]. Moreover, a correction factor of $C_L = 2$ was used in these simulations to account for the quite coarse grid and to consider a worst-case behavior related to dust combustion and flame propagation; lower pressures are expected if a lower correction factor is used. The role played by C_L, alone and in combination with the cell size, has already been studied in [23]. It is expected that further simulations cover more possible scenarios, including different volumes and length-to-diameter ratios, along with other dust cloud sizes.

Although the FLACS-DustEx code has been extensively validated against different sets of experimental data [23,27,43], it is not possible to compare the simulations presented here with experimental results, since no data are available on dust explosions in such a large volume. This desirable comparison would serve to improve the accuracy of the simulations. For that reason, the numerical results presented here should be considered with caution, particularly the comparison of overpressures and vent areas with venting standards. Different $P_{red,sim}$ values would be obtained depending on the levels adopted for each factor. The qualitative trends and relations between parameters could be considered more relevant. It is also important to highlight the limitations that still persist in the dust explosion field [49], including the uncertainties over the dust concentration and turbulence fields in large industrial equipment and the interactions between the different variables and physical phenomena involved.

The results from the factorial analysis indicated that the most relevant parameters in the scenario studied were the vent area, ignition location, and dust concentration, whereas the turbulence level had lower importance. However, the levels of these factors to be considered in CFD simulations should be tailored to each specific scenario considering the real industrial facility and the process conditions.

On the other hand, the interaction turbulence/ignition position might have different origins, but no clear explanation was found; here it is pertinent to remark on the multi-peak nature of venting and the complex interactions between the different physical processes that define each pressure peak, still not fully understood [50].

Although limited, the results in Table 4 do indicate several trends that could have implications for the industry. Firstly, the significant role played by the dust concentration. When the concentration was reduced from 500 g/m^3 to 300 g/m^3, the pressure lowered by 53% on average, i.e., $P_{red,sim}$ halved. This means that the generation and accumulation of fine particles should be addressed. Though the presence of dust is unavoidable during the handling of bulk materials, the amount matters. Therefore, gentle conveying systems that minimize impacts and rubbing or grinding actions are to be preferred [51]. In addition,

installing dust collecting systems throughout the loading and unloading points of the conveying line could decrease the total amount of dust. Additionally, filling systems that reduce product breakage and dust generation in the silo, such as spiral chutes, should be selected. All these measures, which match the principles of inherently safer design [52], can help to mitigate the consequences of a possible explosion accident.

Secondly, the influence of the level of turbulence on $P_{red,sim}$. The lower turbulence level varied $P_{red,sim}$ by -31% on average. Again, the filling system selected for the silo could have an influence here, along with the operational velocity [53].

Thirdly, higher explosion overpressures were obtained when the ignition was located near the bottom of the silo. Controlling where the ignition takes place in the inner volume of the silo is not feasible, but some specific preventing measures can be applied to reduce ignition probability at the base of the silo. To avoid a thermite reaction between a foreign body made of aluminum impacting rusty steel [54], stainless steel could be used to define an impact zone covering the center of the silo floor [11]. Also, all equipment within the silo, including the discharging systems, should be suitable for hazardous areas. Finally, these results have proved that the factorial analysis could be useful, not only for designing lab-scale explosion experiments [55] but also for planning CFD simulations. This methodology could be applied to the assessment of explosion risks in storage facilities, which can integrate CFD simulations [32], and also to the improvement of guidelines and standards on explosion venting.

5. Conclusions

CFD simulations of vented dust explosions in a 4500 m^3 silo for wood pellets were carried out. The influence of the initial turbulence level, dust concentration, ignition location, and vent area on the reduced explosion overpressure was analyzed by defining a set of different study cases. A factorial analysis determined the importance of these variables: 25% for the three latter and 13% for the former. In addition, one interaction effect between ignition location and initial turbulence was detected for the explosion scenario considered in this study, with an additional effect of 5%.

This methodology has proved useful to study detailed situations not specifically contemplated by venting standards and to analyze the effects of initial variables. CFD models combined with factorial analysis could help practitioners to assess explosion risks in industrial storage facilities.

References

1. Eckhoff, R.K. Understanding dust explosions. The role of powder science and technology. *J. Loss Prev. Process Ind.* **2009**, *22*, 105–116. [CrossRef]
2. Klippel, A.; Schmidt, M.; Krause, U. Dustiness in workplace safety and explosion protection—Review and outlook. *J. Loss Prev. Process Ind.* **2015**, *34*, 22–29. [CrossRef]
3. Ilea, C.G.; Kosinski, P.; Hoffmann, A.C. The effect of polydispersity on dust lifting behind shock waves. *Powder Technol.* **2009**, *196*, 194–201. [CrossRef]

4.   Amyotte, P.R.; Eckhoff, R.K. Dust explosion causation, prevention and mitigation: An overview. *J. Chem. Health Saf.* **2010**, *17*, 15–28. [CrossRef]

5.   Eckhoff, R.K. *Dust Explosions in the Process Industries*, 3rd ed.; Gulf Professional Publishing/Elsevier: Amsterdam, The Netherlands, 2003; pp. 20–25.

6.   Abbasi, T.; Abbasi, S.A. Dust explosions—Cases, causes, consequences, and control. *J. Hazard. Mater.* **2007**, *40*, 7–44. [CrossRef]

7.   García Torrent, J.; Ramírez-Gómez, A.; Fernandez-Anez, N.; Medic Pejic, L.; Tascón, A. Influence of the composition of solid biomass in the flammability and susceptibility to spontaneous combustion. *Fuel* **2016**, *184*, 503–511. [CrossRef]

8.   Ferreira, T.; Marques, E.; Monney, J.M.; Pinho, C. A Study on the spontaneous ignition of some ligneous pellets. *Fire* **2023**, *6*, 153. [CrossRef]

9.   Casson Moreno, V.; Cozzani, V. Major accident hazard in bioenergy production. *J. Loss Prev. Process Ind.* **2015**, *35*, 135–144. [CrossRef]

10. Krigstin, S.; Wetzel, S.; Jayabala, N.; Helmeste, C.; Madrali, S.; Agnew, J.; Volpe, S. Recent health and safety incident trends related to the storage of woody biomass: A need for improved monitoring strategies. *Forests* **2018**, *9*, 538. [CrossRef]

11. Coffey, C.J.; Price, D.W. Probabilistic risk assessment in combination with CFD modelling of biomass dust explosions within large bulk storage volumes. In Proceedings of the Hazards XXIII Symposium, Southport, UK, 12–15 November 2012.

12. Siwek, R. Explosion venting technology. *J. Loss Prev. Process Ind.* **1996**, *9*, 81–90. [CrossRef]

13. Yuan, Z.; Khakzad, N.; Khan, F.; Amyotte, P. Domino effect analysis of dust explosions using Bayesian networks. *Process Saf. Environ. Prot.* **2016**, *100*, 108–116. [CrossRef]

14. *EN 14491*; Dust Explosion Venting Protective Systems. European Committee for Standardization: Brussels, Belgium, 2012.

15. *NFPA 68*; Standard on Explosion Protection by Deflagration Venting. National Fire Protection Association: Quincy, MA, USA, 2023.

16. Zalosh, R. *Explosion Venting Data and Modeling—Literature Review*; The Fire Protection Research Foundation: Quincy, MA, USA, 2008.

17. Siwek, R. New revised VDI guideline 3673 "Pressure release of dust explosions". *Process Saf. Prog.* **1994**, *13*, 190–201. [CrossRef]

18. *EN 14034-1*; Determination of Explosion Characteristics of Dust Clouds—Part 1: Determination of the Maximum Explosion Pressure p_{max} of Dust Clouds. European Committee for Standardization: Brussels, Belgium, 2011.

19. *EN 14034-2*; Determination of Explosion Characteristics of Dust Clouds—Part 2: Determination of the Maximum Rate of Explosion Pressure Rise $(dp/dt)_{max}$ of Dust Clouds. European Committee for Standardization: Brussels, Belgium, 2011.

20. Tascón, A. Design of silos for dust explosions: Determination of vent area sizes and explosion pressures. *Eng. Struct.* **2017**, *134*, 1–10. [CrossRef]

21. Tascón, A.; Aguado, P.J.; Ramírez, A. Dust explosion venting in silos: A comparison of standards NFPA 68 and EN 14491. *J. Loss Prev. Process Ind.* **2009**, *22*, 204–209. [CrossRef]

22. Middha, P.; Samaraweera, R.; Coffey, C.; Price, D.W. The Influence of Explosion Relief Vent Layouts on Explosion Overpressures in Large Biomass Storage Vessels. *Chem. Eng. Trans.* **2016**, *48*, 205–210. [CrossRef]

23. Tascón, A.; Aguado, P.J. Simulations of vented dust explosions in a 5 m³ vessel. *Powder Technol.* **2017**, *321*, 409–418. [CrossRef]

24. Proust, C.; Leprette, E.; Snoeys, J. The role of turbulence in explosion vent system design. In Proceedings of the Hazards XXII Symposium, Liverpool, UK, 11–14 April 2011.

25. Tamanini, F. Aspect Ratio Effects in Unvented and Vented Dust Explosions. *Ind. Eng. Chem. Res.* **2012**, *51*, 7636–7642. [CrossRef]

26. Tascón, A.; Ramírez-Gómez, A.; Aguado, P.J. Dust explosions in an experimental test silo: Influence of length/diameter ratio on vent area sizes. *Biosyst. Eng.* **2016**, *148*, 18–33. [CrossRef]

27. Castellanos, D.; Skjold, T.; van Winggerden, K.; Echkoff, R.K.; Mannan, M.S. Validation of the DESC code in simulating the effect of vent ducts on dust explosions. *Ind. Eng. Chem. Res.* **2013**, *52*, 6057–6067. [CrossRef]

28. Klippel, A.; Schmidt, M.; Muecke, O.; Krause, U. Dust concentration measurements during filling of a silo and CFD modeling of filling processes regarding exceeding the lower explosion limit. *J. Loss Prev. Process Ind.* **2014**, *29*, 122–137. [CrossRef]

29. Rani, S.I.; Aziz, B.A.; Gimbun, J. Analysis of dust distribution in silo during axial filling using computational fluid dynamics: Assessment on dust explosion likelihood. *Process Saf. Environ. Prot.* **2015**, *96*, 14–21. [CrossRef]

30. Reding, N.S.; Shiflett, M.B. Consequence prediction for dust explosions involving interconnected vessels using computational fluid dynamics modeling. *J. Loss Prev. Process Ind.* **2020**, *65*, 104149. [CrossRef]

31. Olugbemide, D.I. A CFD study of the effects of pipe bending angle on pressure piling in coal dust explosions in interconnected vessels. *Fire Saf. J.* **2022**, *128*, 103540. [CrossRef]

32. Abuswer, M.; Amyotte, P.; Khan, F.; Imtiaz, S. Retrospective risk analysis and controls for Semabla grain storage hybrid mixture explosion. *Process Saf. Environ. Prot.* **2016**, *100*, 49–64. [CrossRef]

33. Ghaffari, M.; van Wingerden, K.; Gjøvåg Hagen, J.T.; Skjold, T.; Storvik, I. Sensitivity Analysis of Dust Explosion Consequences in a Roller Mill using FLACS-DustEx. *Chem. Eng. Trans.* **2016**, *53*, 157–162. [CrossRef]

34. Tascón, A.; Ruiz, A.; Aguado, P.J. Dust explosions in vented silos: Simulations and comparisons with current standards. *Powder Technol.* **2011**, *208*, 717–724. [CrossRef]

35. Huang, C.; Bloching, M.; Lipatnikov, A.N. A vented corn starch dust explosion in an 11.5 m³ vessel: Experimental and numerical study. *J. Loss Prev. Process Ind.* **2022**, *75*, 104707. [CrossRef]

36. Ogunfuye, S.; Sezer, H.; Kodakoglu, F.; Farahani, H.F.; Rangwala, A.S.; Akkerman, V. Dynamics of explosions in cylindrical vented enclosures: Validation of a computational model by experiments. *Fire* **2021**, *4*, 9. [CrossRef]
37. Feroukas, K.; Chiapolino, A.; Saurel, R. Simplified interfacial area modeling in polydisperse two-phase flows under explosion situations. *Fire* **2023**, *6*, 21. [CrossRef]
38. *FLACS-CFD v22.1r2 User's Manual*; Gexcon: Bergen, Norway, 2022.
39. Launder, B.E.; Spalding, D.B. The numerical computation of turbulent flows. *Comput. Methods Appl. Mech. Eng.* **1974**, *3*, 269–289. [CrossRef]
40. Hjertager, B.H.; Solberg, T.; Nymoen, K.O. Computer modelling of gas explosion propagation in offshore modules. *J. Loss Prev. Process Ind.* **1992**, *5*, 165–174. [CrossRef]
41. Tascón, A.; Aguado, P.J. CFD simulations to study parameters affecting dust explosion venting in silos. *Powder Technol.* **2015**, *272*, 132–141. [CrossRef]
42. Skjold, T.; Arntzen, B.J.; Hansen, O.R.; Taraldset, O.J.; Storvik, I.E.; Eckhoff, R.K. Simulating dust explosions with the first version of DESC. *Process Saf. Environ. Prot.* **2005**, *83*, 151–160. [CrossRef]
43. Skjold, T. Review of the DESC project. *J. Loss Prev. Process Ind.* **2007**, *20*, 291–302. [CrossRef]
44. Hauert, F.; Vogl, A.; Radant, S. Dust cloud characterization and its influence on the pressure-time-history in silos. *Process Saf. Prog.* **1996**, *15*, 178–184. [CrossRef]
45. Dean, A.; Voss, D.; Draguljić, D. *Design and Analysis of Experiments*, 2nd ed.; Springer: Cham, Switzerland, 2017.
46. Montgomery, D.C. *Design and Analysis of Experiments*, 8th ed.; Wiley: Hoboken, NJ, USA, 2013; pp. 255–259.
47. Bartknecht, W. Effectiveness of explosion venting as a protective measure for silos. *Plant/Oper. Prog.* **1985**, *4*, 4–13. [CrossRef]
48. Eckhoff, R.K. Use of $(dP/dt)_{max}$ from closed-bomb tests for predicting violence of accidental dust explosions in industrial plants. *Fire Saf. J.* **1985**, *8*, 159–168. [CrossRef]
49. Skjold, T. Dust explosions modeling: Status and prospects. *Part. Sci. Technol.* **2018**, *36*, 489–500. [CrossRef]
50. Dorofeev, S.B. Flame acceleration and explosion safety applications. *Proc. Combust. Inst.* **2011**, *33*, 2161–2175. [CrossRef]
51. Dafnomilis, I.; Lodewijks, G.; Junginger, M.; Schott, D.L. Evaluation of wood pellet handling in import terminals. *Biomass Bioenergy* **2018**, *117*, 10–23. [CrossRef]
52. Brown, K.R.; Whelan, C.; Murray, G.; Laturnus, B.; Yazdanpanah, F.; Cloney, C.; Amyotte, P. Application of process hazard analysis and inherently safer design in wood pellet production. *ACS Omega* **2022**, *7*, 47720–47733. [CrossRef] [PubMed]
53. Jägers, J.; Wirtz, S.; Scherer, V.; Behr, M. Experimental analysis of wood pellet degradation during pneumatic conveying processes. *Powder Technol.* **2020**, *359*, 282–291. [CrossRef]
54. van Wingerden, K. Mechanical sparks as an ignition source of gas and dust explosions. *Chem. Eng. Trans.* **2019**, *77*, 133–138. [CrossRef]
55. Castellanos, D.; Carreto, V.; Skjold, T.; Yuan, S.; Chaudhari, P.; Mannan, M.S.; Mashuga, C. Construction of a 36 L dust explosion apparatus and turbulence flow field comparison with a standard 20 L dust explosion vessel. *J. Loss Prev. Process Ind.* **2018**, *55*, 113–123. [CrossRef]